LRP 811/05 December 2005

Recent physics results with electron cyclotron heating in TCV

A. Pochelon, S. Alberti, G. Arnoux, Y. Camenen,
E. Fable, A. Mueck, L. Porte and the TCV Team

Invited plenary lecture
6th Int. Workshop on "Strong Microwaves in Plasmas", July 25 - August 1, 2005,
Nizhny Novgorod - St. Petersburg, Russia

ISSN 0458-5895

RECENT PHYSICS RESULTS WITH ELECTRON CYCLOTRON HEATING IN TCV

A. Pochelon, S. Alberti, G. Arnoux, Y. Camenen, E. Fable, A. Mück, L. Porte and the TCV Team

Centre de Recherches en Physique des Plasmas CRPP EPFL,
Association EURATOM-Confédération Suisse,
Ecole Polytechnique Fédérale de Lausanne EPFL,
Switzerland

With its 2nd and 3rd harmonic flexible Electron Cyclotron (EC) system (3MW at 82.7GHz and 1.5MW at 118GHz), adapted to its flexible plasma shaping capabilities, TCV (Tokamak à Configuration Variable) explores a large spectrum of EC heating (ECH) and current drive (ECCD) physics, from low to high plasma densities, that is in different collisionality and confinement regimes. This paper reviews some recent highlights of TCV ECH experiments.

Second harmonic X-mode (X2) radially localized EC heating allows a variation of the normalised electron temperature gradient and electron temperature independently and over a large range. These experiments are dedicated to the separation of the effects of collisionality and plasma shape on electron heat transport.

Third harmonic heating (X3) allows initial exploration of β-limits at intermediate currents and densities. The coupling of the wave is optimised by feedback control of the mirror angle, based on a sinusoidal oscillation of the mirror angle. Since the coupling increases with electron temperature and density, best performance are obtained at the maximum of the available 3rd harmonic power and typically at 3/4 of the cutoff density, around n_{eo}~8-10 $10^{19}m^{-3}$. Central heating of both electron and ion species has been achieved, providing an increase of β from 1 to 2.5%, equivalent with the normalised value β_N=2.

First evidence of EBW (Electron Bernstein Waves) global power absorption and radially localized heating in a tokamak has been obtained in an H-mode plasma. The results have been obtained using the low field side O->X->B-wave conversion scheme which becomes possible at high density (n_{eo}~20-25 $10^{19}m^{-3}$), a density several times overdense to 2nd harmonic O-mode.

The three kind of experiments addressed in this paper can also be seen as a set of experiments at increasingly high densities, using the adequate EC wave propagation mode (X2, X3, EBW) to provide accessibility and power absorption.

EC-System on TCV (X2, X3)

An essential part of the TCV tokamak program is dedicated to the study of the effect of plasma shape on plasma confinement and stability properties, see Fig.1. Electron cyclotron waves (ECW), with a power coupling independ-

ent of the plasma-launcher distance, were therefore the obvious choice. Moreover, the narrow localization of the 2nd harmonic ECW X-mode (X2) power deposition is crucial for transport studies together with current profile and instability control. Third harmonic ECWs (X3), with a three times higher density cutoff, provide access to higher density, allowing the study of β-limits at intermediate currents.

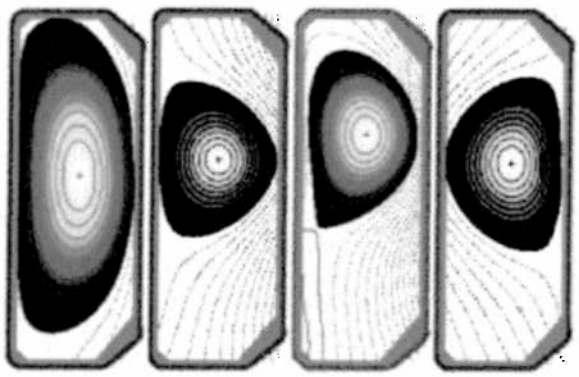

Fig.1. Examples of plasma shapes in TCV

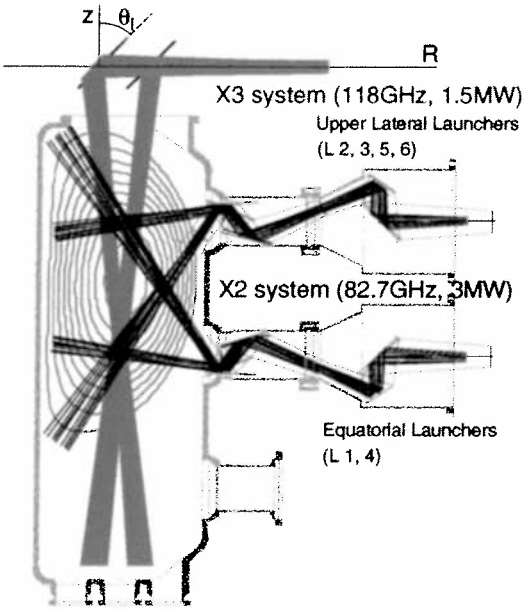

Fig.2 X2 and X3 launchers set-up

The TCV ECW system is composed of six 2nd harmonic X2 gyrotrons with low field side (LFS) launchers (3MW, 2s, 82.7GHz, $n_{e\ \text{cutoff X2}} = 4.3\times10^{19}\text{m}^{-3}$) [1] and three 3rd harmonic X3 gyrotrons using one top launcher (1.5MW, 2s, 118GHz, $n_{e\ \text{cutoff X3}} = 11.5\times10^{19}\text{m}^{-3}$) [2], see Fig.2. All launchers have two degrees of freedom and can be steered in real time. The gyrotrons and matching optical units are separated from the tokamak by about 30m of evacuated waveguides lines of 62.5mm diameter, with a transmission efficiency of typically 95%. In the plasma, a high heating power density can be achieved, up to more than 30MW/m^3 with central X2 injection. The relative alignment of the different X2 launcher mirrors is accomplished using the highly localised sawtooth period response at the q=1 resonant surface [3]. The main codes relevant for this paper are, TORAY-GA for ray tracing, [4], ART for the conversion to electron Bernstein waves [5], Fokker-Planck CQL3D for the non-linear CD (X2&X3) [6], the inverse equilibrium code LIUQE [7] and CHEASE [8].

Access to high density with EC Waves

The accessibility of EC waves depends primarily on the magnetic field. We compare the accessibility of EC waves in different machines, from the low field spherical tokamaks or compact tori (B=0.5T), through the rather low field TCV (B=1.5T, R=0.88m, a=0.25m), to the high field ITER machine (5.3T). The accessibility limitation due to EC cutoffs is compared to the specific machine plasma density limit, given by the empirical Greenwald density limit $\langle n_{eG}\rangle = 0.27\ I_p/a^2$ [9]. The nominal ITER operation parameters are taken as a reference, also standard for the other machines envisaged, namely: safety factor q_{95}=3, elongation $\kappa = 1.85$ and triangularity $\delta = 0.5$, with $q_{95} \sim (5a^2B_o/R_oI_p)\cdot f(a/R)\cdot[1+\kappa^2(1+2\delta^2+\ldots)]/2$. The typical ratios of *EC cutoffs* versus *machine* accessible density range, $n_{e\ cutoff}/n_{eoG}$, are given (%) in Fig.3 for these conditions.

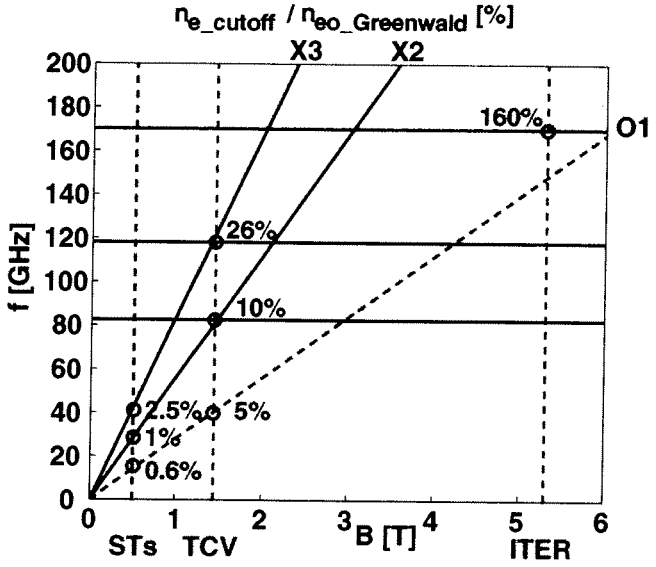

Fig.3. Ratio of EC cutoff density to Greenwald density limit for different gyrotron frequencies and magnetic fields (in %).

In ITER, the field is sufficiently high to allow for the heating of the complete machine density range with the fundamental O-mode (O1) at 170GHz. In spherical tokamaks however, the lowest harmonics ECWs allow only for the heating of up to a few percent of n_{eG}, thus justifying the great hopes placed in the potential of EBWs, which exhibit no principle high-density limit. In the medium field machine TCV, 10% of n_{eG} is accessible with the 2nd harmonic X-mode (X2), a range extended to 26% with the use of the 3rd harmonic X-mode (X3). The density range above X3 accessible densities could be accessed with 2nd harmonic EBWs.

If current drive using EBWs would develop in addition to heating, then there are potential applications of EBW even in high a field machine like ITER.

Electron Heat Transport with Shape & Collisionality

Increasing the energy confinement in order to limit the amount of additional heating needed for a reactor grade plasma is one of the big tasks in tokamak research. Plasma shape is one of the free parameters, which influences transport and confinement.

The effect of plasma shape on core electron heat transport in low-density L-mode plasmas is investigated in TCV using strong localized EC heating to vary both the electron temperature T_e and the normalized electron temperature gradient R/L_{Te} [10-12]. The power is deposited at two radial locations, see Fig.4, one off-axis just outside the q=1 surface, at ρ_1, and the other far off-axis, at ρ_2, a radius still guaranteeing full first-pass absorption. The power ratio $P(\rho_1)/P(\rho_2)$ essentially determines the electron temperature gradient, whereby the total power strongly influences T_e at mid-radius, the radius of investigation, by determining the total heat flux at the edge. Varying the two

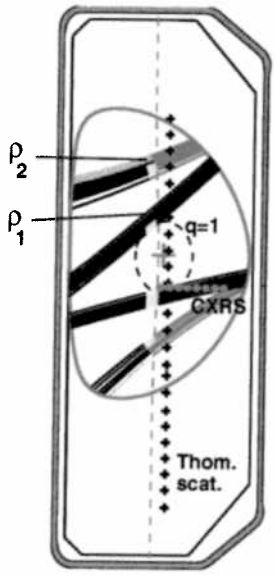

Fig.4. EC beams for off-axis (ρ_1) and far off-axis deposition (ρ_2), with the positions of the cold EC resonance, q=1 surface, Thomson and CXRS diagnostics measurements.

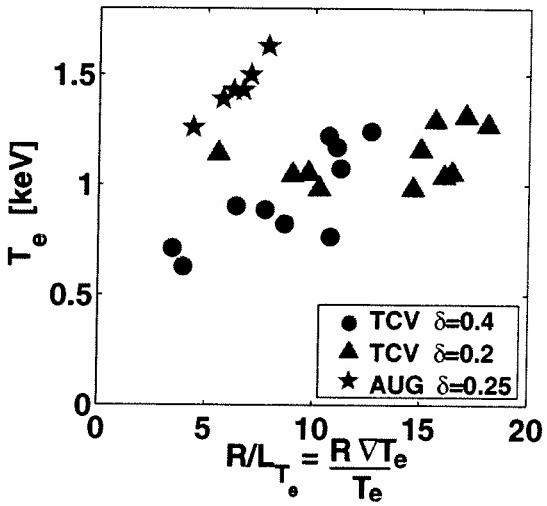

Fig.5. Range of T_e and R/L_{Te} explored in TCV and AUG. In TCV, T_e and R/L_{Te} are varied independently.

parameters $P(\rho_1)/P(\rho_2)$ and P_{tot} independently allows decoupling R/L_{Te} and T_e, see Fig.5. The large EC power available in TCV allows exploring a range of R/L_{Te} three times larger than in preceding similar studies [13]. To study the effect of plasma shape, the triangularity was varied from negative to positive values, $-0.4<\delta<+0.4$. The strong modification of the edge pedestal and stabil-

ity with triangularity in H-mode [14] justifies the use of L-mode in a first study of the direct effect of plasma shape on core heat transport.

Typical parameters at mid-radius are T_e=0.6-1.3keV, T_e/T_i=2-4, R/L_{Te}=4-20, Z_{eff}=2-5, ν_{eff}=0.25-1, where $\nu_{eff}= \nu_{ei}/\omega_{De}\sim 0.1Rn_e^{19}Z_{eff}/T_e^2$, the collision frequency versus curvature drift frequency, is the effective collisionality relevant for micro-instabilities [15]. Simulations with the local gyro-Landau fluid code GLF23 [16] and with the global collisionless linear gyro-kinetic code LORB5 [17] show that with such parameters, trapped electron modes (TEM) are the most unstable modes, except for the very lowest values of R/L_{Te}, where ion temperature gradient (ITG) modes dominate. In addition to the effect of plasma shape, the experimental study focuses on the dependences of χ_e on T_e, R/L_{Te} and ν_{eff}, plasma parameters predicted to strongly influence TEM stability.

The experimental electron heat diffusivity χ_e is found to increase strongly with the electron temperature, with no strong dependence on R/L_{ne} or R/L_{Te}, from the whole parameter range explored, Fig.6. This result is obtained at constant n_eZ_{eff}. The strong dependence of χ_e on T_e suggests a gyro-Bohm and/or a collisionality dependence.

Looking more into the details of the R/L_{Te} dependence, it appears from Fig.7 that for R/L_{Te}>8, the gyro-Bohm heat diffusivity does not depend on R/L_{Te}, while at R/L_{Te}<8, TCV data are compatible with ASDEX Upgrade (AUG) data showing an increase of $\chi_e/T_e^{3/2}$ with R/L_{Te}.

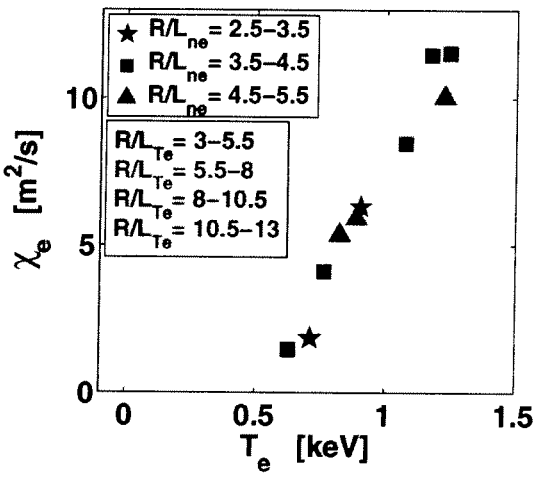

Fig.6. Strong dependence of χ_e versus T_e at mid-radius, despite a large range of variations in R/L_{ne} and R/L_{Te}.

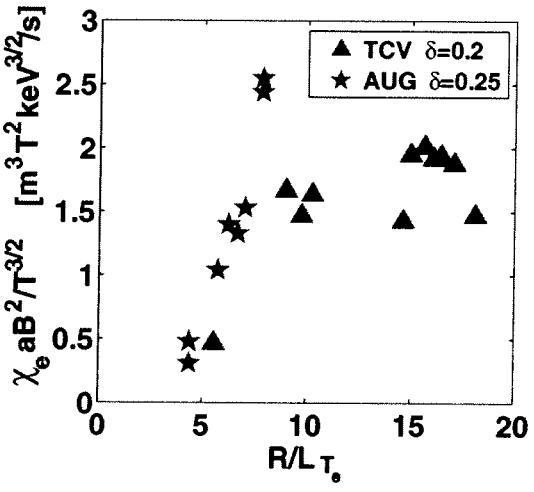

Fig.7. Gyro-Bohm normalized electron heat diffusivity χ_e versus normalized electron temperature gradient.

The effect of plasma triangularity on electron heat diffusivity – in these TEM dominated plasmas – can first be illustrated by a specific example, which represents well the effect of triangularity on local and on global transport properties. In the experiment depicted in Fig.8, the heating power just outside the q=1 surface was adapted to get at the negative triangularity δ=-0.4 the same T_e-profile than the one obtained at the positive triangularity δ=+0.4 with 1.35MW. The other parameters, n_e, Z_{eff}, q_{95} being held constant, it turns out that less than half of the power was needed at negative triangularity, compared to positive triangularity. At the negative triangularity comparatively to the positive triangularity, the (global) confinement time and confinement time enhancement factor are increased, respectively τ_{Ee}=3.6->7.7ms and H_{RLW}=1.5->1.9; and the (local) heat diffusivity from power balance is decreased, $\chi_e^{PB}(\rho=0.5)$=8.5->2.6 m^2/s, with similar trend from heat pulse analysis.

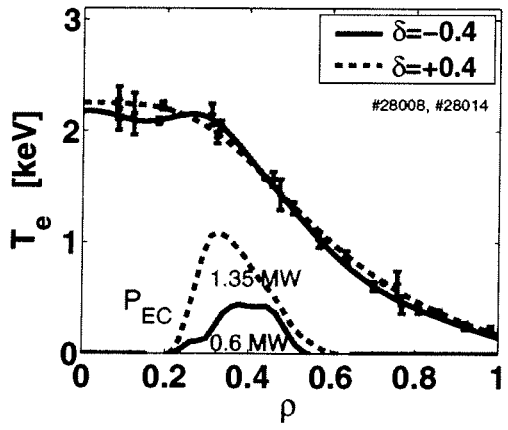

Fig.8. Identical T_e profiles obtained at negative triangularity δ=-0.4, as compared to positive triangularity δ=+0.4, with half the EC power.

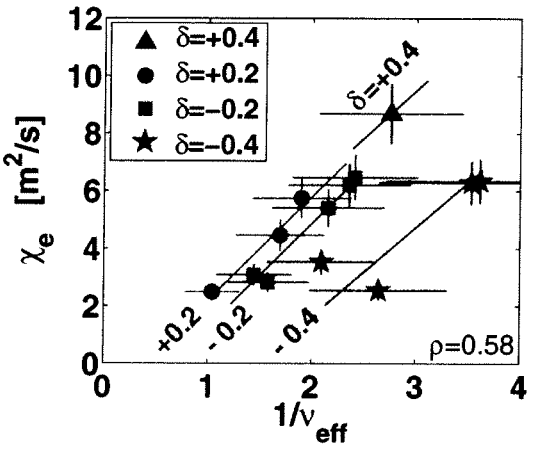

Fig.9. Separation of shape and collisionality effects, both influencing χ_e. (q_{95}=const.)

Comparing the data with different values of n_eZ_{eff}, it appears that χ_e does not only depend on T_e, but also on n_eZ_{eff} and that the heat diffusivity and the gyro-Bohm normalised heat diffusivity decrease strongly with increasing effective collisionality. The finding of a reduction of electron heat transport with ν_{eff} is consistent with ASDEX Upgrade experimental results [18] and with the predicted stabilising effect of ν_{eff} on the TEM modes, as shown e.g. from GLF23 simulations.

The coupled effect of plasma triangularity and collisionality is shown in Fig.9. The heat diffusivity does not vary significantly from δ=0.4 to δ=0.2. However, at negative triangularity, χ_e clearly decreases with decreasing δ. For the whole range of triangularity, χ_e decreases strongly with increasing ν_{eff}.

Thus, the present experiments have allowed us to separate the effect of plasma shape – here the triangularity - and collisionality on local electron heat transport. Small and negative triangularity, as well as low effective collisionality have both been shown to reduce favourably the electron heat transport, in this TEM dominated regime. Although the reason of the effect of plasma triangularity needs still to be determined, the strong effect on electron heat transport may be used as a tool to ease or control the access to electron internal transport barriers (eITB).

X3 Heating for high β in H-mode

In the moderate magnetic field of TCV, the recently installed X3 system broadens the tokamak operational range, providing the possibility of heating plasmas at high density, well above the X2 cutoff density [19, 20]. To compensate for the significantly weaker absorption in X3 compared to the absorption in X2, top-launch injection is used to maximise the ray path along the resonance layer, with a shallow incidence on the resonance, thus maximising the optical depth.

The X3 mirror is located on top of TCV vacuum vessel (as shown in Fig.2) and collects the power of three gyrotron beams. It is steerable both along the major radius ($0.8<R<0.96$m) from pulse to pulse and azimuthally ($40^\circ<\theta<50^\circ$) during discharges, with a maximum speed of $d\theta/dt=20^\circ/s$. A key characteristic of the X3 top launch is the high sensitivity of the absorption on the mirror angle θ. In a typical L-mode plasma ($n_{eo}=4\ 10^{19}m^{-3}$, $T_{eo}=2.7$keV), the maximum power absorbed is typically 40-60% with a FWHM $\Delta\theta\sim1.4^\circ$. For a plasma with fixed n_e and T_e profiles, ray-tracing calculations show that the optimum mirror angle (at fixed mirror radius R) depends sensitively on the central density ($d\theta/dn_{eo}=0.18^\circ/(n_{eo}10^{19}m^{-3})$, due to refraction) and central temperature ($d\theta/dT_{eo}=0.2^\circ$/keV, due to the relativistic shift). There are additional effects from the Shafranov shift and the paramagnetic cold resonance displacement ($\sim I_p^2$). This high sensitivity to the mirror angle has motivated the development of a real time control of the mirror angle.

The real-time control is based on a sinusoidal modulation of the mirror angle and a synchronous demodulation of the soft X-ray plasma response. With this system it is possible to generate an error signal proportional to $dI_X/d\theta$ (or $dT_{eX}/d\theta$ in Fig.10) where $dI_X/d\theta$ is obtained from a central soft X-ray chord passing through plasma axis. The error signal is proportional to the slope $dI_X/d\theta$. In the closed loop system, this error signal is compared to an externally preset reference, and the difference between the error signal and the reference is fed to a PID controller. The dynamic response of the closed-loop system with a PI controller is shown in Fig.10 where the external preset

mirror angle was fixed at a value of 45.5 °. After a transient period of approximately 250ms the error signal vanishes. This real-time feedback is fully operational in L-mode plasmas, where up to full single-path absorption has been measured (DML) for plasma densities lower than 4 $10^{19}m^{-3}$. At these plasma densities the calculated absorbed power fraction (TORAY) based on the assumption of a Maxwellian distribution function, is found to be significantly lower than the measured one, a difference due to the presence of the suprathermal electrons generated by the X3 heating itself.

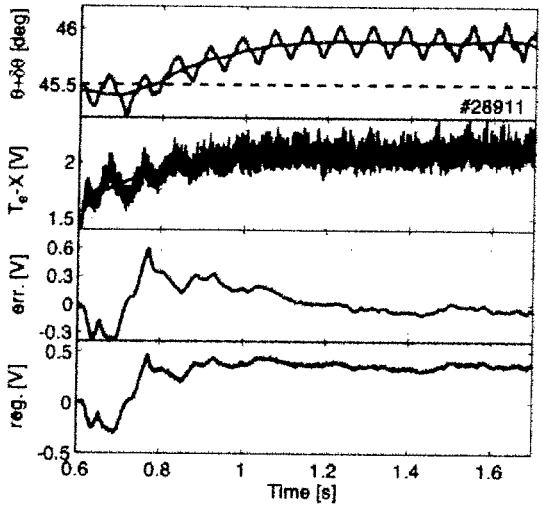

Fig.10. X3 mirror angle feedback closed loop response. Preset (dashed) and optimal mirror angle with 13Hz superimposed mirror oscillations, maximizing the soft X-ray T_{eX}, together with error and regulation signals.

In H-mode plasmas, due to the presence of the strong ELM perturbations, the present feedback system is not yet operational. However, the improved confinement in H-modes improves sufficiently the absorption that the need for a feedback system is less stringent.

In recent experiments dedicated to the heating of H-mode plasmas with the full installed X3 power (1.35MW), it has been possible to reach quasi-full power absorption in a plasma with central density n_{eo}~8 $10^{19}m^{-3}$, owing to the electron temperature increase from 0.8 to 2.5keV soon after heating start, leading to an increase of the absorbed power P_{abs} from 28 in Ohmic to 94% with X3 heating on.

The temporal evolution of the relevant parameters is shown in Fig.11. At the full X3 power level, an ELMy regime fundamentally different to Ohmic/low-power-heating ELMy H-mode has been found (with large ELMs of lower frequency or small "grassy" ELMs). The presence of these ELMs allows establishing a stationary H-mode at constant density. The plasma energy increases by more than a factor two, with a very substantial increase of the ion temperature, due to collisions at these high densities.

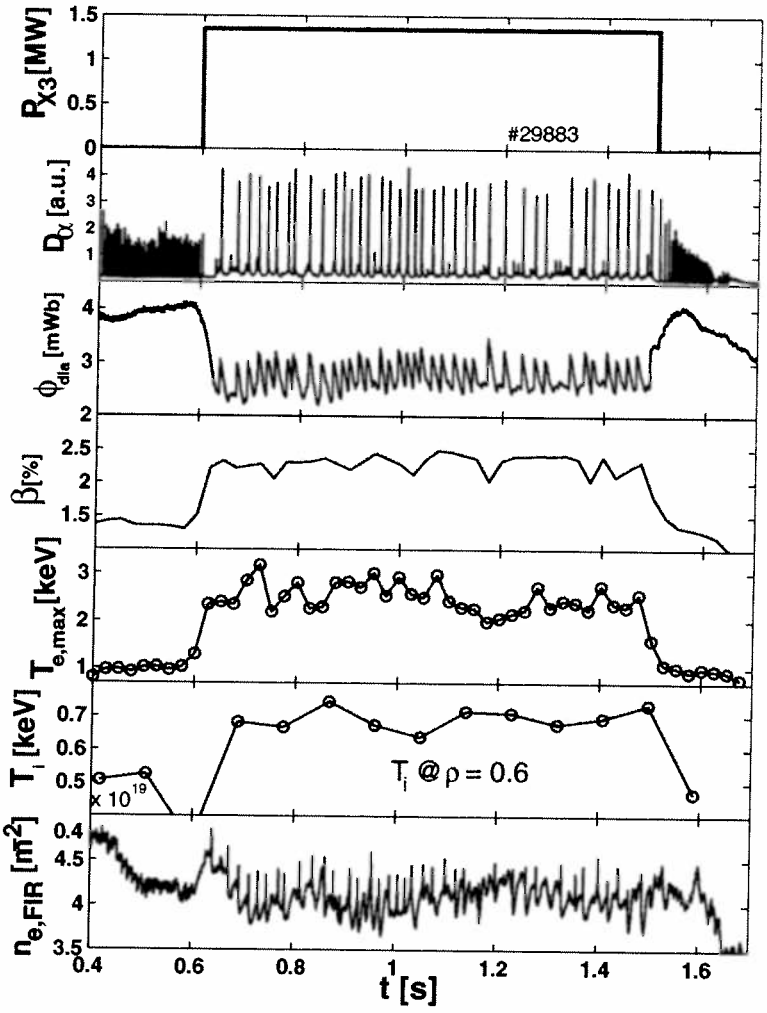

Fig.11. β increase with X3 heating in H-mode. From top to bottom: X3 power, D_α showing ELM behaviour change, diamagnetic flux, total plasma β, Thomson scattering central T_{eo}, ion temperature at ρ=0.6 from CXRS, line integrated density.

With the applied heating, the plasma β increases from 1 to β_{max}=2.4%, with up to a normalised beta $\beta_N = \beta[\%]/I_N[\text{mT/MA}] = 2$ (with $I_N = I/aB \sim 1.25$ [MA/mT]), typically 3/4 of the ideal MHD Troyon pressure limit, see Fig.12. Long stationary discharges, which are MHD stable can be obtained, but the large ELMs in these low q discharges can degrade the core confinement instantaneously [21].

Encouraged by these results, we are presently studying the possibility of upgrading the installed X3 power on TCV by increasing the unit power of each existing gyrotron by approximately 30% (~600kW/gyrotron) and by adding a fourth gyrotron with a LFS injection. In total, this upgrade would allow to nearly double the X3 power coupled to the plasma in X3.

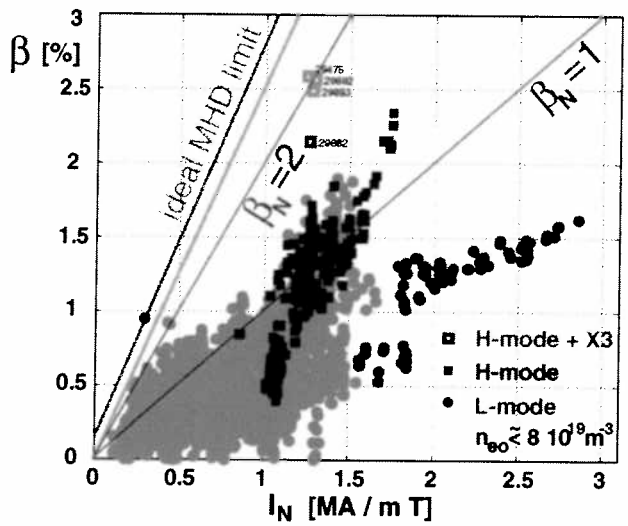

Fig.12. β enhancement with X3 full power heating in TCV H-modes. The recent X3 heated H-modes (empty squares) reach a normalised beta β_N~2, a sizable fraction of the ideal MHD Troyon pressure limit [21], also shown.

Electron Bernstein Wave Heating in TCV

Electron Bernstein Waves offer the possibility of heating low-field machines like spherical tokamaks or tokamaks with EC waves at densities far above the conventional cutoff density of O- and X-modes [22]. The first demonstration of EBWH on a torus took place on a stellarator. Bernstein waves heating can be of particular interest in low field tokamaks ($B \leq 3$-4T), where the conventional EC cutoffs are typically lower than the Greenwald density limit.

With a low field side (LFS) launch, overdense plasmas are accessible through the double mode conversion O-X-B scheme. This scheme combines two advantages: it uses an oblique launch, minimising the risk of power reflection to the gyrotron, and permits coupling to Bernstein waves through a low-density path accessible to conventional O- and X-modes.

The refraction bends the oblique O-mode wave ray path until it nearly parallels the magnetic field lines, where O-X conversion occurs, and from where the wave propagates back towards the upper hybrid layer. The O-X conversion transmission function, as a function of toroidal (z) and poloidal (x) refractive index is [23]:

$$T(N_x,N_z) = \exp(-\pi k_0 L_{ne}\ \mathrm{sqrt}(Y/2)\ [2(1+Y)(N_{z,opt}-N_z)^2 + (N_x^2)])$$

with $Y=\omega_{ce}/\omega$

Thus, a large transmission angular conversion window requires 1) a high-density gradient, or small density scale length L_{ne}, 2) a central density n_{eo} above O-mode cutoff. The subsequent X-B conversion occurs naturally in a hot plasma close to the upper hybrid resonance layer. The converted B-wave propagates further to the centre where it is dissipated at the EC resonance harmonic. A typical O-X-B mode conversion ray path is shown in Fig.13.

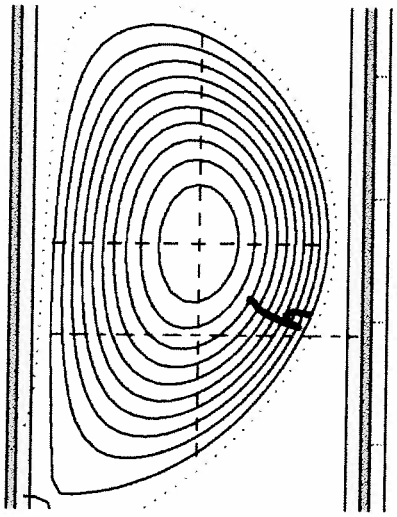

Fig.13. Typical ray path in poloidal projection of an O->X->B wave conversion, launched from an equatorial TCV port (height indicated by the lower dotted line). The plasma magnetic axis is above equator (12cm).

A low q_{95}~2.3 Ohmic H-mode target plasma was developed (I_p=400kA, κ=1.8, δ=0.55), with a slowly rising density, exhibiting ELMy and ELM-free phases, with adequate high edge density gradients. The heating studies [24] use a central density of 1.5 $10^{19}m^{-3}$, typically half of the Greenwald density limit.

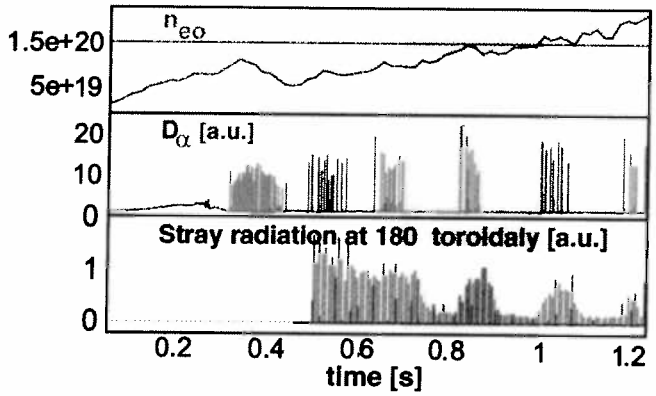

Fig.14. ELMy H-mode with ELM-free phases, with density evolution, D_α-emission, and strong absorption (low EC stray radiation) during ELM-free periods.

Prior to heating experiments, the value of the correct O-mode injection angles needs first to be determined. It has been noticed that the power of one gyrotron beam (0.47MW) is influencing the H-mode properties, triggering ELMs or enhancing the D_α-emission with a delay of the order of 1-2ms, associated with a simultaneous decrease of the power conversion. Therefore, to determine the angular conversion-absorption window without perturbing the H-mode, the power was injected in relatively short pulses at low power duty cycle (6%). The level of EC stray radiation, monitored at 180° toroidally, gives a measure of the converted power, see Fig.14. The stray radiation is found to be low, i.e. indicates good absorption, when the angle is set close to the expected optimal angle, and decreases asymptotically during the establishment of an ELM free phase.

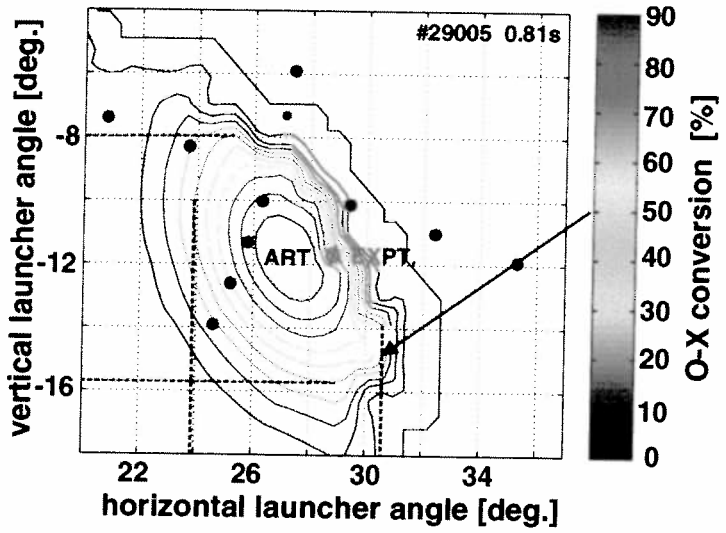

Fig.15. Optimum angular absorption response (EXPT) from two experimental angular scan (dots) compare well with ART calculation (within 2 degrees).

A two-directional scan of the injection angle, searching for the minimum of the stray radiation around the presumed optimal angle, yields the optimal launcher angle position through interpolation. This experimental angle overlaps, within a 2° error, with the optimal angle determined from the ray tracing code ART [5], as shown in Fig.15. This small difference is compatible with the uncertainty in the equilibrium reconstruction. In addition, the experimental window (15-20° FWHM) appears larger than the calculated one (8° FWHM), which can be due to the uncertainty in the n_e-profile determination in the region of the steep density gradient.

With a higher duty cycle, the total power absorbed is measured from the modulated energy via the diamagnetic probe. A power of more than 60% of the injected O-mode power has been measured, as shown in Fig.16.

With X-mode injection instead, there is no significant absorption, less than 10%, or with a knowingly wrong injection angle, the same measurement yields a very small-absorbed power.

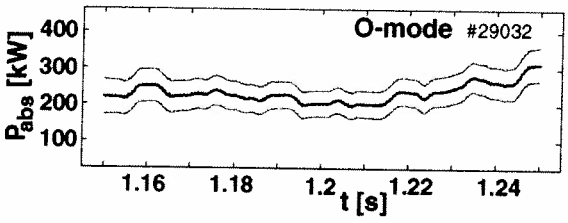

Fig.16. Global power absorption in O->X->B conversion from the diamagnetic probe: a) the power absorbed, b) phase of DML signal vs. modulation.

Local power deposition is found on the soft X-ray DMPX wire-chamber camera, directly from the evolution of the soft X-ray emission at the heating pulse, as well as from Fourier transform, at a location close to the predicted power deposition from the ART code.

These high power EBH experiments demonstrate both local and global absorption of EBW wave using the O-X-B scheme in a conventional aspect ratio tokamak, in good agreement with the simulations.

Conclusions

Using the flexibility of TCV plasma shaping and the capability of varying the electron temperature and gradients with high power and localised second harmonic EC heating, it is possible to separate the independent effects of plasma shape and collisionality on electron heat transport. In these dominant trapped electron mode regimes, low and negative triangularity as well as high collisionality reduce electron heat transport.

In the moderate magnetic field TCV, third harmonic ECH X3 heating has allowed successful heating of H-mode plasmas approaching a sizeable fraction of the β-limit and demonstrating at the same time full power absorption of the X3 microwave power. At these high densities, the direct heating of the electrons by the ECWs and the indirect heating of the ions through collisions with the electrons both contribute to the plasma performance.

To add here for information, plasma scenarios in which the 2^{nd} and 3^{rd} harmonic EC heating systems can usefully be combined have been developed in TCV. This is the case for example in low current high elongation discharges, in which the 2^{nd} harmonic X2 is used to increase the vertical stability margin through broadening of the current profile, while the plasma core, overdense to X2, is heated using the 3^{rd} harmonic X3 [26].

For the first time in an overdense plasma of a conventional aspect ratio tokamak, EBWH, relying on the O-X-B mode conversion scheme, has been recently demonstrated in TCV, launching second harmonic waves from the LFS. This mode conversion scheme requires a steep density gradient at the plasma edge and a density overdense to O-mode, which both can be satisfied in TCV Ohmic H-modes. The optimal launcher injection angles were determined experimentally from the EC stray radiation and compare well with ray tracing calculation. A global deposition exceeding 60% of the launched power was so far measured from the diamagnetic probe, and only within the prescribed conversion angular window. This heating can typically be useful in low field devices, where the conventional EC cutoffs are limiting the operation to density values well below the Greenwald density limit.

Acknowledgements

This work was partly supported by the Swiss National Science Foundation.

References

1. Goodman T.P. et al., Proc. 19th SOFT, 1966, Lisbon, **I**, 565.
2. Hogge J.-Ph. et al., Nucl. Fus., 2003, **43**, 1353.
3. Angioni C. et al., Nucl. Fus., 2003, **43**, 455.
4. Matsuda K., IEEE Trans. Plasma Sci., 1989, **17**, 6.
5. Volpe F., Laqua H.P. et al., Rev. of Sci. Instrum., 2003, **74**, 1409.
6. Harvey R.W., et al., *Proc. IAEA Tech. Conf. on Advanc. in Simul. and Modell. of Thermonucl. Plasmas*, Montreal 1992, (IAEA, Vienna, 1992).
7. Hofmann F., Tonetti G., Nucl. Fus., 1998, **28**, 1871.
8. Lütjens H., et al., *Computer Physics Comm.*, 1996, **97**, 219.
9. Greenwald M. et al., Nucl. Fus., 1998, **28**, 2199.
10. Camenen Y. et al., 32nd EPS Plasma Phys. Conf., Tarragona 2005, P1.052.
11. Camenen Y. et al., Plasma Phys. Control. Fusion, 2005, **47**, 1971.
12. Pochelon A., Camenen Y. et al., 20th IAEA Fusion Energy Conf., Vilamoura 2004, IAEA-CN-116/EX/9-1.
13. Ryter F. et al., Nucl. Fus., 2003 **43**, 1396.
14. Saibene G. et al., Plasma Phys. Control. Fusion, 2002, **44**, 1769.
15. Angioni C. et al., Phys. of Plasmas, 2003, **10**, 3225.
16. Dorland W. et al., Phys. of Plasmas, 1997, **4**, 2482.
17. Bottino A., et al., Phys. of Plasmas, 2004, **11**, 198.
18. Ryter F. et al., Phys. Rev. Lett., 2005, **95**, 085001.
19. Arnoux G. et al., Plasma Phys. Control. Fusion, 2005, **47**, 295.
20. Alberti S. et al., IAEA TM ECRH, Como 2005, accept. in J. Phys.: Conf. Series.
21. Porte L. et al., 19th IAEA Fusion Energy Conf., Lyon 2002, IAEA-CN-94/EX/P5-15.
22. Troyon F. et al., Plasma Phys. Controlled Fusion, 1984, **26**, 209.
23. Preinhaelter J. and Kopecky V., J. Plasma Physics, 1973, **10**, 1.
24. Mjølhus A. et al., Plasma Phys., 1984, **31**, 7.
25. Mück A., et al., 32nd EPS Plasma Phys. Conf., Tarragona, 2005, P4.410.
26. Pochelon A. et al., 19th IAEA Fusion Energy Conf., Lyon 2002, IAEA-CN-94/EX/P5-14.